

# Intraalloy Electron Transfer and Catalyst Performance: A Spectroscopic and Electrochemical Study

John B. Goodenough\* and R. Manoharan

Center for Materials Science and Engineering, ETC 5.160, The University of Texas at Austin, Austin, Texas 78712-1084

A. K. Shukla and K. V. Ramesh

Solid State and Structural Chemistry Unit, Indian Institute of Science, Bangalore 560012, India

Received August 15, 1988

The synergistic promotion of three important fuel cell reactions on Pt-Ru electrodes suggests that electron transfer from ruthenium to platinum within the alloy may be responsible. Spectroscopic evidence for such a charge transfer is presented, and its consequences are analyzed not only for three fuel cell reactions, oxygen reduction and hydrogen and methanol oxidation, but also for two electrolytic reactions, hydrogen and oxygen evolution. It is pointed out that although a modest electron transfer in an alloy enhances the reactions synergistically, too large a charge transfer binds surface species adsorbed from the electrolyte too tightly to allow the reactants access to the electrode surface. This latter phenomenon is demonstrated on a Ni-Ti electrode, which is inactive for all three fuel cell reactions. However, Ni-Ti is stable in acid and gives normal electrolytic reactions, but with onset potentials and exchange-current densities lowered or raised in predictable directions. Chronopotentiograms for oxygen evolution and methanol oxidation reactions on 75-25 Pt-Ru electrodes are interpreted; they support the prediction that charge transfer enhances the adsorption of oxygen species from the electrolyte to the surface, which is the rate-limiting step in methanol oxidation.

## Introduction

A synergistic catalytic activity has been reported for Pt-Ru alloys used as electrodes in fuel cell<sup>1-13</sup> and other<sup>14</sup> electrochemical reactions. Previous speculation on the origin of this synergistic promotion has considered only the hydrogen evolution reaction,<sup>15</sup> we emphasize here the 3d electron transfer from one atomic species to another in a binary transition-metal alloy, and we present a general discussion of its consequences for surface-catalyzed electrochemical reactions.

We first argue that in the Pt-Ru alloys there is an electron charge transfer from the ruthenium to neighboring platinum atoms, and we present XPS, EXAFS, and ESR data on Pt-Ru alloy catalysts that support this assertion. We then consider the influence such a charge transfer would have on five technically important reactions: the electroreduction of oxygen and the electrooxidation of

hydrogen and of methanol, which are of interest for fuel cell technology, and the electrolytic evolution of hydrogen and oxygen. We argue that a modest charge transfer can synergistically enhance the fuel cell reactions but that too large a charge transfer must suppress them. On the other hand, the electrolytic reactions are not suppressed, but their onset potentials and exchange-current densities are raised or lowered in predictable directions. This argument is supported by studies on a 50-50 Ni-Ti electrode.

These several predictions are tested electrochemically. These experiments include chronopotentiograms for the oxygen evolution and methanol oxidation reactions that reveal a reduction, in the alloy, of the critical field strength across the double layer for attracting to the surface an oxygen species from the aqueous electrolyte.

## Experimental Section

**(a) Pt-Ru Catalysts.** High-surface-area carbon substrate was prepared from coconut shell by the method described previously.<sup>16</sup> In this method, activated carbon is comminuted by heating in carbon dioxide atmosphere at 900 °C. Different compositions of Pt-Ru alloy catalysts were prepared by impregnating the carbon substrate with 2 wt % aqueous chloroplatinic acid and 1 wt % ruthenium chloride in diluted HCl. This was followed by reduction with 5 wt % boiling sodium formate solution. The coated substrate particles were then washed with copious amounts of boiling distilled water.

**(b) Ni-Ti Alloy.** The 50-50 ordered Ni-Ti alloy used in this study was a disk cut from a commercially obtained sheet.

**(c) Preparation of Pt-Ru/C Electrodes.** The details of electrode preparation are described elsewhere.<sup>17</sup> In brief, the electrodes were prepared by hot pressing (140 °C) the catalyzed substrate on platinum-metal screens (0.06-mm-diameter wire, 1024 mesh cm<sup>-2</sup>) at ca. 55 kg/cm<sup>2</sup> of pressure with 20 wt % polyethylene as binder.

(1) Niedrach, L. W.; Mckee, D. W.; Paynter, J.; Danzig, I. F. *Electrochem. Technol.* 1967, 5, 318.

(2) Barbier, J.; Lamy, E.; Outiki, O. *React. Kinet. Catal. Lett.* 1981, 18, 127.

(3) Stonehart, P. *Adv. Hydrogen Energy* 1982, 3, 1149.

(4) Petry, O. A.; Podlovchenko, B. I.; Frumkin, A. N.; Lal, H. *J. Electroanal. Chem.* 1965, 10, 253.

(5) McNicol, B. D.; Short, R. T. *J. Electroanal. Chem.* 1977, 81, 249.

(6) McNicol, B. D.; Short, R. T. *J. Electroanal. Chem.* 1978, 92, 115.

(7) Andrew, M. R.; McNicol, B. D.; Short, R. T.; Drury, J. S. *J. Appl. Electrochem.* 1977, 7, 153.

(8) Watanabe, M.; Motoo, S. *J. Electroanal. Chem.* 1975, 60, 267.

(9) Watanabe, M.; Suzuki, T.; Motoo, S. *Denki Kagaku* 1970, 38, 927.

(10) Watanabe, M.; Uchida, M.; Motoo, S. *J. Electroanal. Chem.* 1986, 199, 311.

(11) Tamura, K.; Tsukui, T.; Kamo, T.; Kudo, T. *Hitachi Hyoson, Enerugi Shingijutsu* 1984, 66, 49.

(12) Rao, K. V.; Roy, C. B. *Adv. Electrochem. Energy Storage Conversion, Proc. Symp. Karaikudi, India, 1983*, 3.1.

(13) Goodenough, J. B.; Hammett, A.; Kennedy, B. J.; Manoharan, R. *J. Electroanal. Chem.* 1988, 240, 133.

(14) Anderson, J. R. *Structure of Metallic Catalysts*; Academic Press: New York, 1975.

(15) Jaksic, M. M. *J. Mol. Catal.* 1986, 38, 161.

(16) Ramesh, K. V. Ph.D. Thesis, Indian Institute of Science, Bangalore, 1986. Shukla, A. K.; Ramesh, K. V.; Manoharan, R.; Vasudevan, S. *Ber. Bunsen-Ges. Phys. Chem.* 1985, 89, 1261.

(17) Kannan, A. M.; Shukla, A. K.; Hammett, A. *J. Appl. Electrochem.* 1988, 18, 149.

(d) **Electrochemical Measurements.** Steady-state galvanostatic polarization data were obtained with a conventional three-electrode cell having a glass separator between the working and counter electrodes, regulated dc power supply, and high-power decade resistance box in series with the electrochemical cell. Chronopotentiograms and cyclic voltammograms were obtained from EG&G Headstart Creative Electrochemistry Software.

(e) **Physicochemical Characterization.** All  $K\alpha$  X-ray photoelectron spectra (XPS) were obtained at 30 °C with a VG Scientific Ltd. ESCA-3 Mark II spectrometer. The vacuum in the chamber was better than  $10^{-9}$  Torr. The Ru(3p) and Pt(4f) signals were analyzed by comparing the spectra of the catalyst samples with those of the pure Ru and Pt metals obtained under identical conditions. The spectra of the catalyst samples were considerably broader than those of the pure metals; with a least-squares procedure<sup>16</sup> it was possible to fit the broadened spectra by introducing several components each with a line shape identical with that of the pure metal.

Extended X-ray absorption fine structure spectra (EXAFS) were obtained at 30 °C with a Siemens single-crystal spectrometer;<sup>16</sup> the (200) plane of a LiF single crystal was used as the analyzer. Electron spin resonance (ESR) spectra were recorded at 30 and -140 °C for several catalyst samples with a Varian-109 spectrometer. X-ray powder diffraction patterns were obtained at room temperature on a JEOL powder diffractometer, and electron micrographs were taken with a JEOL-200 high-resolution electron microscope. The extent of dispersion of the active metal and the total surface area were estimated by hydrogen chemisorption and nitrogen BET measurements with a Micromeritics Accusorb-2100E.

The catalyst samples studied were exposed to the air after preparation and during handling for spectral analysis; no special precautions were taken to store the samples in an inert or reducing atmosphere.

## Results and Discussion

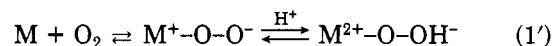
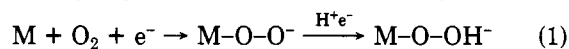
**1. Chemical Consequences of Charge Transfer. (a) General Considerations.** The essential consequences of charge transfer for the catalytic activity of an alloy surface are well illustrated by the following important reactions: oxygen reduction, hydrogen oxidation, methanol oxidation, and hydrogen and oxygen evolution. Each of the first three reactions requires that the reactants other than the electrolyte, have access to the catalyst surface; the final two involve only reactions between the catalyst and the electrolyte. If intermediate species adsorbed from the electrolyte are too tightly bound to the catalyst surface at the potentials where the first three reactions occur, then they block access to the surface by the reactant and suppress these three reactions. The synergistic influence of a promoting solute would thus appear to be its influence on the surface binding energy of the blocking species.

Charge transfer between elements of a binary alloy introduces an electrostatic bias into the surface bonding of an adsorbate. At the more electropositive element M, species containing oxygen are more tightly bound and protons tend to be repelled; at the more electronegative element  $\bar{M}$ , protons are more tightly bound and species containing oxygen are more easily displaced. The greater the charge transfer in an alloy, the more tightly bound are the adsorbed reaction intermediates adsorbed from the electrolyte.

Experimentally, introduction of Ru into Pt has been shown to promote oxygen reduction, hydrogen oxidation, and methanol oxidation as well as to suppress formation of oxygen species on Pt but not on Ru. We will argue that in the Pt-Ru system, charge transfer from Ru to Pt promotes the rate-limiting step of these three reactions without suppressing access of the reactants  $H_2$ ,  $O_2$ , and  $CH_3OH$  to the surface. In the case of Ni-Ti, charge transfer stabilizes the nickel against corrosion in acid media,<sup>18-21</sup> presumably the titanium suppresses formation

of oxygen species on the neighboring nickel atoms while binding oxygen species strongly to itself. Conversely, hydrogen is more tightly bound to the nickel and more easily repelled from titanium sites. Since maximum d-electron charge transfer is anticipated for a 50-50 ordered alloy between Ti and Ni, two first-row transition elements from opposite ends of the 3d series, it is of interest to determine whether adsorbed species won from the aqueous electrolyte are bound so strongly they inhibit access of the reactants  $H_2$ ,  $O_2$ , and  $CH_3OH$  to the alloy surface.

(b) **Oxygen Reduction.** As pointed out by Yeager,<sup>22</sup> oxygen reduction may take place by either a direct four-electron pathway or a peroxide pathway. The four-electron pathway has been observed with chelates such as platinum phthalocyanine.<sup>23,24</sup> However, at a metal or alloy surface, the peroxide pathway appears to be the dominant reaction mode. In this reaction, dioxygen reacts with the surface by first accepting an electron from the catalyst:



where reaction 1 is electrochemical and 1' is purely chemical. In either case, the chemisorbed species is negatively charged, it is therefore electrostatically bound to the surface if the reaction is chemical. However, if the reaction is electrochemical, the electrostatic component of the force between the chemisorbed species and the surface will depend upon the applied voltage and the net intrinsic charge on the surface atom. In an element the intrinsic charge is neutral; in a transition-metal alloy d-electron transfer from the constituent to the left in the periodic table makes this constituent effectively more positive as the empty d states become acceptors of the oxygen lone-pair electrons. For a given voltage, a d-electron charge transfer would make the constituent more attractive to a negatively charged surface species. In a Pt-Ru alloy, for example, an oxygen species would be more tightly bound to a surface Ru atom; in the alloy, Ru thus acts as a promoter of reaction 1 provided the reactant  $O_2$  is not blocked from the  $M = Ru$  surface atoms by an oxygen-species adsorbate.

Two reaction pathways are available for the next critical step in the reduction process:



where step 2 is electrochemical and step 2' is chemical. In an alloy, the more electropositive surface atom (to which the oxygen species is attached) provides an electrostatic force that favors the desired electrochemical pathway relative to the chemical reaction. Thus the electrochemical step 2 (eq 2) should be enhanced in an alloy by a d-electron charge transfer from species M to species  $\bar{M}$ . Moreover, the preference of oxygen for the Ru sites in an alloy—even in the chemical reaction of step 1'—is consistent with the XPS, EXAFS, and ESR evidence for retention of oxide species on the Ru sites but for their suppression on the Pt sites. Reaction 2 is promoted more strongly by a larger

(18) Bhattacharya, R. S.; Pronko, P. P.; Rai, A. K.; McCormick, A. W.; Raffoul, C. N. *Nucl. Instrum. Methods Phys. Res.* **1985**, *B7/8*, 694.

(19) Bhattacharya, R. S.; Raffoul, C. N.; Rai, A. K. *Corrosion* **1986**, *42*, 236.

(20) Mitsuhashi, A.; Asami, K.; Kawashima, A.; Hashimoto, K. *Corros. Sci.* **1987**, *27*, 957.

(21) Manoharan, R.; Goodenough, J. B., unpublished results.

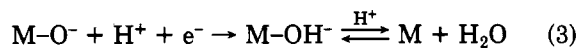
(22) Yeager, E. J. *Mol. Catal.* **1986**, *38*, 5.

(23) Paliteiro, C.; Hamnett, A.; Goodenough, J. B. *J. Electroanal. Chem.* **1984**, *160*, 359.

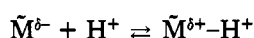
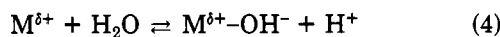
(24) Shukla, A. K.; Paliteiro, C.; Manoharan, R.; Hamnett, A.; Goodenough, J. B. *J. Appl. Electrochem.* **1989**, *19*, 105.

charge transfer; if this step is rate-limiting, it shifts the optimum alloy composition to less than 50 at. % Ru.

The final steps in the electrochemical reduction of oxygen are straightforward—and generally not rate-limiting—on either the elemental or the alloy catalysts:

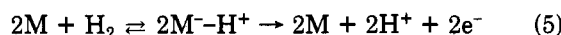


However, too large a d-electron charge transfer would shift the rate-limiting step to reaction 3 by making it more difficult for an O<sub>2</sub> molecule to displace the final product species of electrochemical reaction 3 from the surface; once the rate-limiting step is shifted to (3), any further charge transfer would lower the overall activity of the surface for oxygen reduction. For example, oxygen reduction does not occur on the surface of a 50–50, ordered Ni–Ti alloy (see below). We interpret this result to be a demonstration that the O<sub>2</sub> reactant does not have access to the surface because electron transfer from Ti to Ni has attracted from the electrolyte tightly bound reaction intermediates:



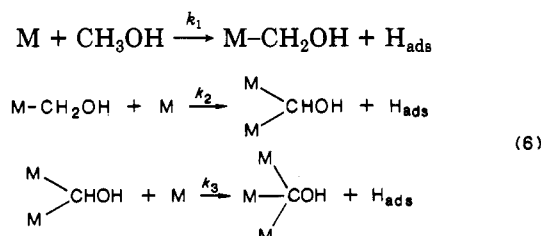
that are not displaced by O<sub>2</sub> at the potential for the oxygen-reduction reaction.

**(c) Hydrogen Oxidation.** In the hydrogen oxidation reaction, dihydrogen first reacts with the surface of the catalyst by donating two electrons to it:

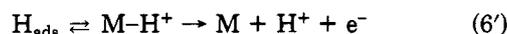


so the chemisorbed species is positively charged. In the second, electrochemical step of the reaction, charge transfer from one atomic species to another in an alloy introduces an extra electrostatic energy to the binding energy. This extra component is attractive at the more electronegative species  $\tilde{\text{M}} = \text{Pt}$ ; it is repulsive at the more electropositive species  $\text{M} = \text{Ru}$ . The rate-limiting step of the overall reaction is the electrochemical second step, i.e., the separation of the electronic charge trapped at the surface from the bound proton. A repulsive electrostatic component would promote this second step, which is consistent with Ru acting as a promoter of the overall reaction on the Pt–Ru alloys. The smaller work function of Ru means that the hydrogen is less tightly bound at elemental Ru than at elemental Pt, which shifts the optimum alloy composition to greater than 50 at. % Ru. On the other hand, reaction 4 apparently blocks access of the reactant H<sub>2</sub> to the surface of Ni–Ti (see below).

**(d) Methanol Oxidation.** In the case of methanol oxidation, three quite different electrochemical reactions must occur. The first is a dissociative chemisorption of the alcohol onto the surface, which involves successive donation of electrons to the catalyst:



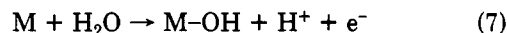
where  $k_1 < k_2 < k_3$  makes M<sub>3</sub>COH the major surface species. H<sub>ads</sub> is lost to the solution as H<sup>+</sup>:



In a Pt–Ru alloy, Ru would promote the initial steps of this reaction in the same way it promotes the hydrogen-

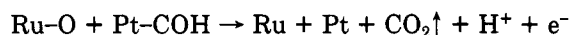
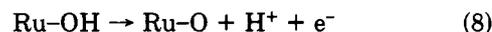
oxidation reaction (eq 5). However, capture of the surface protons and the COH<sup>-</sup> radical<sup>25–27</sup> by negatively charged surface atoms  $\tilde{\text{M}}$  would inhibit their desorption. In the case of Ni–Ti, reaction 4 also blocks access of the reactant CH<sub>3</sub>OH to the surface.

The second electrochemical reaction involves attraction of an oxygen species from the aqueous electrolyte to the catalyst surface:



This reaction is driven by an electric field across the double layer. At a Pt–Ru alloy surface, d-electron charge transfer from Ru to Pt at the surface would reduce the applied voltage required to attract the oxygen species to the surface at a more electropositive Ru atom. Minimization of the applied voltage required for this step is critical for the methanol oxidation reaction.

The third and final electrochemical reaction is the two-step process



in which the first step is promoted by charge transfer from Ru to Pt in the alloy. However, the chronopotentiograms presented in the next section indicate that the rate-limiting step is reaction 7, which would shift the optimum alloy composition to less than 50 at. % Ru as in the oxygen reduction reaction. This analysis is consistent with the observation of Conway<sup>28</sup> that Ru is the more oxophilic element in Pt–Ru alloys.

In contrast to the reactions discussed thus far, hydrogen and oxygen evolution do not require displacement of a surface species by a reactant molecule; therefore, the chemical reaction 4 need not suppress these reactions. On the other hand, charge transfer alters the adsorbate bond strength as well as the free energy of activation  $\Delta G_m$  for the chemical reaction. Therefore we can anticipate a shift in the onset potential as well as a change in the exchange-current density  $i_0 \sim \exp(-\Delta G_m/RT)$ .

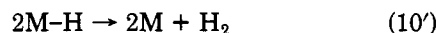
**(e) Hydrogen Evolution.** Hydrogen evolution from acid on a metal surface occurs by the following process: the Volmer reaction



is followed by either the Heyrovsky mechanism



or the Tafel recombination mechanism



The Tafel mechanism requires surface mobility of the adsorbed hydrogen. In an alloy, the hydrogen is preferentially adsorbed at the electron-acceptor element  $\tilde{\text{M}}$ —reaction 4—and its surface mobility may be inhibited, but not suppressed, by this constraint. Therefore hydrogen evolution occurs on the alloy, but the potential at which H<sub>2</sub> evolves, whether by reaction 10 or 10', is shifted to a more negative value by the interelement electron transfer, and an increase in  $\Delta G_m$  would lower the exchange-current density  $i_0$ .

**(f) Oxygen Evolution.** Oxygen evolution begins with a preoxidation step; in acid it is generally reaction 7, but on an alloy this step would be replaced by the chemical

(25) Willsan, J.; Heitbaum, J. *J. Electroanal. Chem.* 1985, 185, 181.

(26) Willsan, J.; Wolter, O.; Heitbaum, J. *J. Electroanal. Chem.* 1985, 185, 163.

(27) Capon, A.; Parsons, R. *J. Electroanal. Chem.* 1973, 45, 205.

(28) Conway, B. E. In *Electrodes of Conductive Metallic Oxides, Part B*; Trasatti, S., Ed.; Elsevier: Amsterdam, 1981; p 633.

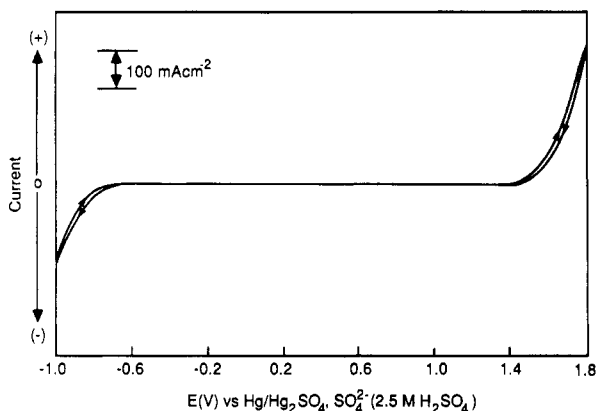


**Figure 1.** Cyclic voltammograms in 2.5 M H<sub>2</sub>SO<sub>4</sub> at 30 °C for a Ni-Ti alloy. Scan rate 100 mV/s. No change was observed in the presence of streaming H<sub>2</sub> or O<sub>2</sub> or after the addition of 1 M CH<sub>3</sub>OH.

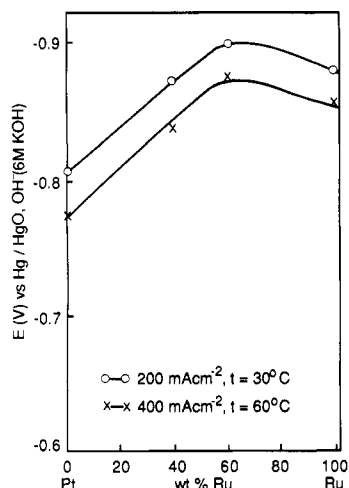
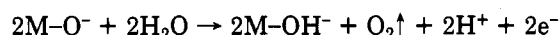
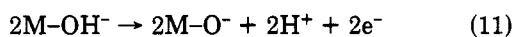
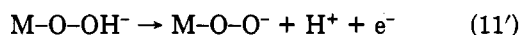
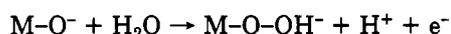


**Figure 2.** Variation with alloy composition of activities at 30 and 60 °C for hydrogen oxidation on polyethylene-bonded carbon-supported Pt-Ru alloy electrodes.

reaction 4. The preoxidation step is followed by a four-electron process by either the recombination mechanism



or, in the absence of surface-oxygen mobility, by



Electron transfer from M to  $\tilde{\text{M}}$  would reduce the surface-oxygen mobility, thereby inhibiting pathway 11, but it should promote pathway 11'; for either pathway it should lower the overpotential for oxygen evolution.

## 2. Electrochemical Results. (a) Oxygen Reduction.

Ramesh et al.,<sup>16</sup> in a galvanostatic polarization study, showed that the maximum performance for oxygen reduction on Pt-Ru alloys in 6 M KOH at 30 °C occurs at the 40-60 Pt-Ru composition.

The room-temperature cyclic voltammogram of Figure 1, obtained in 2.5 M H<sub>2</sub>SO<sub>4</sub>, remains unchanged on the introduction of streaming O<sub>2</sub>, which indicates that oxygen reduction is suppressed on a Ni-Ti electrode.

**(b) Hydrogen Oxidation.** The activity for hydrogen oxidation in 6 M KOH versus alloy composition is shown

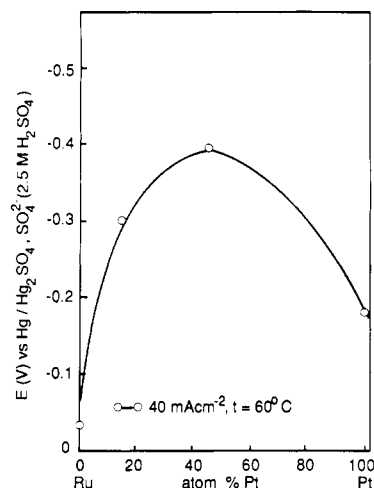


**Figure 3.** Variation with alloy composition at 60 °C for methanol oxidation on Pt-Ru alloy electrodes.

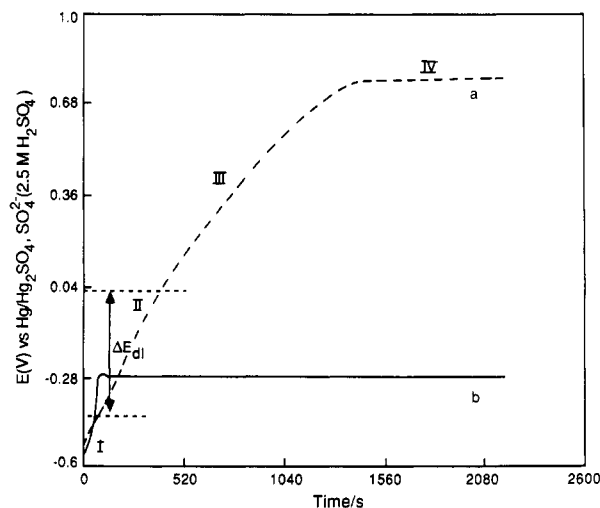


**Figure 4.** Chronopotentiograms of 70-30 Pt-Ru alloy in 2.5 M H<sub>2</sub>SO<sub>4</sub> at 60 °C (a) in the absence and (b) in the presence of 1 M CH<sub>3</sub>OH.

in Figure 2 for Pt-Ru electrodes at both 30 and 60 °C. The activity is here defined as the observed potential for a fixed load-current density. At both temperatures, the maximum activity is found for this reaction also with a 40-60 Pt-Ru electrode. Niedrach et al.<sup>1</sup> have also observed a similar trend in activity for Pt-Ru electrodes.

From Figure 1, no hydrogen oxidation could be seen in the cyclic voltammograms of Ni-Ti even after the introduction of streaming H<sub>2</sub>.

**(c) Methanol Oxidation.** The activity at 60 °C for methanol oxidation in 2.5 M H<sub>2</sub>SO<sub>4</sub> versus alloy composition is shown in Figure 3 for Pt-Ru electrodes. For this reaction, the maximum activity for a current density of 40 mA cm<sup>-2</sup> occurs at the 55-45 Pt-Ru composition. For load currents higher than 100 mA cm<sup>-2</sup>, the optimal alloy composition shifts to 70-30 Pt-Ru.

The chronopotentiograms of Figure 4 record the evolution with time of the potential of a 70-30 Pt-Ru electrode in 2.5 M H<sub>2</sub>SO<sub>4</sub> (a) without and (b) with 1 M CH<sub>3</sub>OH measured from the onset time of a constant anodic current density of 80 mA cm<sup>-2</sup>. The cell was precycled to -650 mV versus a Hg/Hg<sub>2</sub>SO<sub>4</sub>, SO<sub>4</sub><sup>2-</sup> reference electrode before the constant current was applied.

Four distinct time domains can be distinguished in the chronopotentiogram of Figure 4a taken in the absence of methanol: domain I represents the electrochemical oxidation of adsorbed hydrogen from the surface; domain II

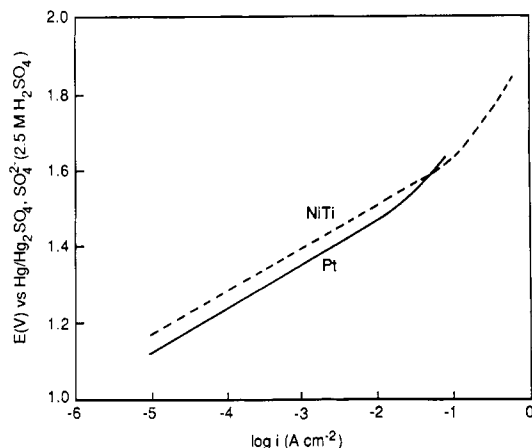
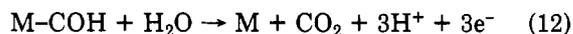


**Figure 5.** Tafel curves for  $O_2$  evolution on Ni-Ti and Pt electrodes at 30 °C in 2.5 M  $H_2SO_4$ .

corresponds to a Faradaic reaction and a charging of the double-layer capacitance occurring simultaneously (a "leaky" capacitor); the Faradaic component consists of oxygen species attracted to the surface from the electrolyte by the electric field across the double layer; in domain III dioxygen formation and electrochemical separation of hydrogen from the chemisorbed oxygen species are occurring; in domain IV dioxygen is evolved from the surface. Similar chronopotentiograms have been reported for oxygen evolution in acid from a Pt electrode.<sup>29</sup>

The chronopotentiogram taken in the presence of methanol (Figure 4b) shows three time domains: the initial slope of the curve represents the electrochemical oxidation of adsorbed hydrogen from the surface, but it is accompanied in this case by adsorption of methanol until the surface becomes poisoned with carbonaceous residues; this brief time domain is followed by a more abrupt drop in potential on charging the double layer; the evolution of  $CO_2$  in the region of constant potential marks the completion of the oxidation reaction. The critical potential at which reaction 7 occurs is located within domain II of chronopotentiogram a, which implies that either a reaction such as



is replacing (7) or that the Faradaic component—the "leak" of the double-layer capacitance—within domain II of the chronopotentiogram of Figure 4a is due to the onset of reaction 7 within this domain. We believe the latter interpretation is the more plausible.

Significantly, the potential drop within domain II for both chronopotentiograms varies with Ru concentration in the Pt-Ru alloys; in each case it is a minimum at the optimum concentration 70–30 Pt-Ru for the overall reaction. This observation is consistent with the assumption that reaction 7 is the rate-limiting step and that it is promoted in the alloy by an electron transfer from Ru to Pt atoms.

At a Ni-Ti electrode, the cyclic voltammogram obtained in 2.5 M  $H_2SO_4$  is no different from that shown in Figure 1 after the addition of 1 M  $CH_3OH$ ; the oxidation of methanol is also suppressed on Ni-Ti.

**(d) Hydrogen Evolution.** Machida et al.,<sup>30</sup> Gutjahr et al.,<sup>31</sup> and Miles<sup>32</sup> have shown that Ni-Ti alloys can be used

(29) Devanathan, M. A. V.; Bockris, J. O'M.; Mehl, W. J. *Electroanal. Chem.* **1959**, *1*, 143.

(30) Machida, K.; Enyo, M.; Toyoshima, I.; Miyahara, K.; Kai, K.; Suzuki, K. *Bull. Chem. Soc. Jpn.* **1983**, *56*, 3393.

(31) Gutjahr, M. A.; Buchner, H.; Beccu, K. D. *Power Sources Symposium*, Brighton, 1972.

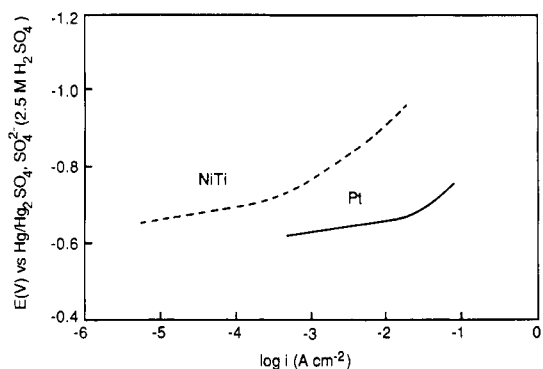


**Figure 6.** Tafel curves for  $H_2$  evolution on Ni-Ti and Pt electrodes at 30 °C in 2.5 M  $H_2SO_4$ .

as cathode materials for hydrogen evolution in alkaline solution. The cyclic voltammogram of Figure 1 shows that the hydrogen evolution reaction also occurs on Ni-Ti in acid. Logarithmic current-potential curves obtained for Ni-Ti and Pt in 2.5 M  $H_2SO_4$  at 30 °C with a flowing  $H_2$  stream in the electrolyte are shown in Figure 5. A Tafel slope of 30 mV/decade, corresponding to a one-electron process with transfer coefficient  $\alpha = 1/2$ , was found for both Ni-Ti and Pt. The results for Pt agree with the accepted literature data.<sup>33</sup> As anticipated in our discussion, the exchange-current density for Ni-Ti ( $10^{-6}$  A  $cm^{-2}$ ) is lower than that for Pt ( $\sim 4 \times 10^{-4}$  A  $cm^{-2}$ ). Literature<sup>34,35</sup> values for the exchange-current densities of elemental Pt and Ru are, respectively,  $\sim 10^{-3}$  and  $\sim 3 \times 10^{-4}$  A  $cm^{-2}$  in 1 N  $H_2SO_4$ . Pt-Ru electrodes with low Pt content show the same performance as pure platinum.<sup>34</sup>

**(e) Oxygen Evolution.** Brooman and Hoar<sup>36</sup> have reported galvanostatic polarization studies of oxygen evolution on anodes of Pt-Ru, Pt-Ir, Pt-Rh, and Pt-Pd alloys. The onset of oxide formation and the overpotential for the evolution of oxygen were lower than on pure Pt for each set of alloys, with Pt-Ru exhibiting the lowest overpotential. No explanation for this synergistic effect was offered at that time.

The cyclic voltammogram of Figure 1 shows that the oxygen evolution reaction occurs in acid electrolyte on the Ni-Ti electrode. Logarithmic current-potential curves obtained for Ni-Ti and Pt electrodes in 2.5 M  $H_2SO_4$  at 30 °C are shown in Figure 6. Both electrodes had to be anodically preelectrolyzed to obtain a well-defined Tafel plot. A Tafel slope of 120 mV decade<sup>-1</sup> was found for both Ni-Ti and Pt, in good agreement with the literature,<sup>37,38</sup> and a four-electron process with  $\alpha \approx 1/2$ . The measured exchange-current densities were  $1.2 \times 10^{-10}$  A  $cm^{-2}$  for Ni-Ti and  $6.9 \times 10^{-10}$  A  $cm^{-2}$  for Pt.

**3. Charge Transfer from Ru to Pt.** The electro-negativity values<sup>39</sup> of ruthenium and platinum metals are 2.11 and 2.22, respectively. Consequently, in a Pt-Ru alloy the Pt and Ru d states interact with each other so as to reflect a net d-electron transfer from the more electropositive Ru atoms to the neighboring Pt atoms; the bonding

(32) Miles, M. H. *J. Electroanal. Chem.* **1975**, *60*, 89.

(33) In *Instrumental Methods in Electrochemistry*; The Southampton Electrochemistry Group; Ellis Harwood: Chichester, 1985.

(34) Bagotsky, V. S.; Skundin, A. M.; Tuseeva, E. K. *Electrochim. Acta* **1976**, *21*, 29.

(35) Bockris, J. O'M.; Reddy, A. K. N. *Modern Electrochemistry*; Plenum Press: New York, 1970; Vol. 2.

(36) Brooman, E. W.; Hoar, T. P. *Platinum Met. Rev.* **1965**, *9*, 122.

(37) Hoare, J. P. *The Electrochemistry of Oxygen*; Wiley: New York, 1968.

(38) Burke, L. D. In *Electrodes of Conductive Metallic Oxides, Part A*; Trasatti, S., Ed.; Elsevier: Amsterdam, 1980; p 141.

(39) Trasatti, S. *J. Electroanal. Chem.* **1971**, *33*, 351.

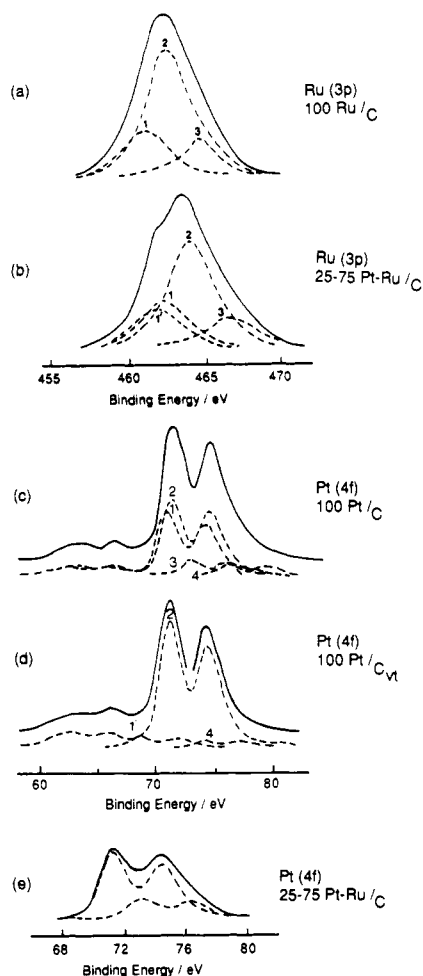


**Figure 7.** XPS spectra of (a) the Ru(3p) region for carbon-supported ruthenium, (b) the Ru(3p) region for carbon-supported 25–75 Pt–Ru alloy, (c) the Pt(4f) region for carbon-supported platinum prior to heat treatment in a vacuum at 500 °C, (d) the Pt(4f) region for carbon-supported platinum after heat treatment in a vacuum at 500 °C, and (e) the Pt(4f) region for carbon-supported 25–75 Pt–Ru alloy; the broken lines show the analyzed spectra labeled with possible species.

states of the narrow d bands have a higher Pt partial density of states, the antibonding states a higher Ru partial density of states. Interatomic charge transfer within the broad s bands would be much smaller.

The maximum charge donated from a Ru atom to its neighboring Pt atoms occurs where the Ru atom has only Pt near neighbors; the maximum charge acceptance by a Pt atom occurs where the Pt atom has only Ru near neighbors. The maximum charge transfer would therefore be found in a 50–50 ordered alloy containing two interpenetrating subarrays of transition-metal atoms from, respectively, the left-hand and the right-hand sides (e.g., group IV and group VIII) of the periodic table. In a disordered alloy system such as Pt–Ru, the optimum composition for a given chemical reaction may be shifted from the 50–50 composition, especially if a rate-limiting reaction is more active on one of the elemental end members.

Figure 7, parts a and b, compares the X-ray photoelectron spectra (XPS) from the Ru(3p) region for two carbon-supported catalysts, elemental Ru and a 25–75 Pt–Ru alloy. The Ru(3p) spectrum for the alloy is shifted to a higher binding energy by about 1 eV relative to that from elemental Ru; this shift represents direct evidence for an electron transfer from Ru in the alloy. The Ru(3d) signal could not be used because it overlaps with the C(1s) signal of the carbon substrate.

Analysis of the XPS spectra gives three Ru(3p) contributions: component 1 may be assigned to metallic Ru and components 2 and 3 to oxides of ruthenium. Prior to the analysis of the spectra into various possible species of ruthenium, the recorded spectra were corrected for background signals with an iterative, self-consistent procedure.<sup>40</sup> The Ru(3p) peaks for elemental Ru and Ru(IV) oxides have been reported to occur at 461.1 and 462.7 eV, respectively.<sup>41</sup> Component 3 in Figure 4a, which is centered at 465 eV, apparently comes from a surface Ru atom in a higher oxidation state, e.g., Ru(V), as has already been reported by Kötzt et al.<sup>41</sup> Comparison of the spectra in Figure 2a,b shows that, for the alloy, the three Ru(3p) components are somewhat better resolved and the oxidized Ru species are not suppressed.

Figure 7, parts c and d compares the spectra of the Pt(4f) region for carbon-supported catalysts containing elemental Pt prior to and after being subjected to heat treatment in a vacuum at 500 °C. The spectrum in Figure 7c shows two dominant sets of doublets—corresponding to species 1 and 2—with binding energies of 70.9, 73.9 eV and 71.3, 74.7 eV, respectively; the values for species 2 are close to the binding energies of  $71.1 \pm 0.05$  and  $74.3 \pm 0.4$  eV of pure platinum metal.<sup>42</sup> The ratio of the areas under the peaks, Pt(4f<sub>5/2</sub>):Pt(4f<sub>7/2</sub>), is close to the expected value of 1.33. Species 1, placed slightly lower than species 2 in the analyzed spectrum, could arise from finely divided elemental platinum occurring in close proximity to carbon. Such shifts are known to occur for the active species in strong metal-support interaction (SMSI) catalysts.<sup>43</sup> The remaining two doublets—corresponding to the species 3 and 4—occur at the binding energies of 72.9, 76.2 eV and 74.1, 79.1 eV, respectively; these may be assigned to oxidized platinum species.

After the vacuum anneal, the spectrum (Figure 7d) shows an absence of species 1 and 3 and the appearance of a new doublet, labeled as 1', at the binding energies of 68.7, 72 eV. In this sample, species 2 is the predominant peak and species 1 is completely absent. Figure 7e shows the spectrum in the Pt(4f) region of a carbon-supported 25–75 Pt–Ru alloy catalyst obtained after “stripping” the Ru(4s) signal. It is similar to the spectrum of Figure 7d; species 1 is totally suppressed in the alloy. Due to the difficulties associated with stripping the Ru(4s) signal, a negative shift of the Pt(4f) spectrum could not be observed, and it is difficult to attribute any significance to the peaks occurring at the binding energies similar to species 3 in the spectrum of Figure 7c.

In light of these difficulties, we supplemented the XPS data with the EXAFS and ESR data of the corresponding catalyst specimens. Figure 8 compares the Fourier transform of the EXAFS spectra for a carbon-supported Pt catalyst prior to and after heat treatment in a vacuum at 500 °C. Comparison of the spectra with model compounds of platinum suggests the presence of only metallic platinum in the catalyst sample that was subjected to heat treatment in a vacuum (Figure 8b), whereas two oxidized platinum species as well as metallic platinum are present in the catalyst that had not been subjected to heat treatment in vacuum (Figure 8a). For comparison, the Fourier transform EXAFS spectrum of a carbon-supported catalyst containing 25–75 Pt–Ru (Figure 9) shows the

(40) Sarma, D. D. Ph.D. Thesis, Indian Institute of Science, Bangalore, 1981.

(41) Kötzt, R.; Lewerenz, H. J.; Stucki, S. *J. Electrochem. Soc.* **1983**, *130*, 825.

(42) Bearden, J. A.; Burr, A. F. *Rev. Mod. Phys.* **1967**, *39*, 125.

(43) Tausser, S. J.; Fung, S. C.; Baker, R. T. K.; Horsley, J. A. *Science* **1981**, *211*, 1121, and the references therein.

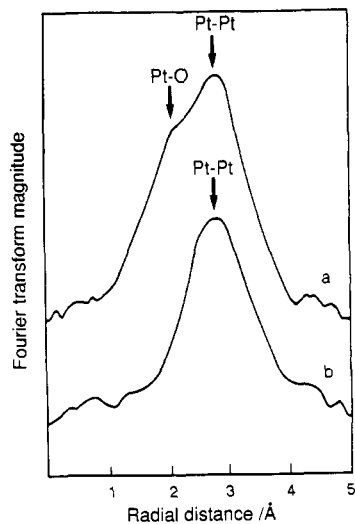


**Figure 8.** Fourier transforms of the EXAFS for carbon-supported platinum (a) prior to and (b) after heat treatment in a vacuum at 500 °C.

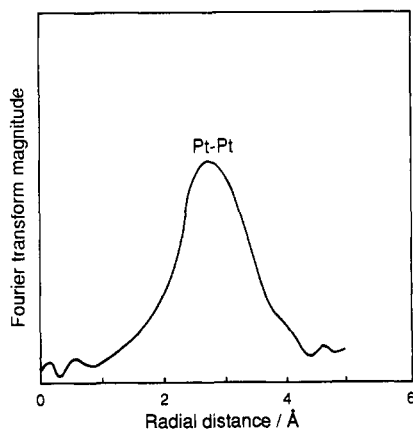


**Figure 9.** Fourier transform of the EXAFS for carbon-supported 25-75 Pt-Ru alloy.

presence of platinum metal alone, which is similar to the situation observed for the vacuum-heat-treated, carbon-supported Pt catalyst. We conclude that the oxidized platinum species normally present on elemental platinum are strongly suppressed on the alloy.

The ESR spectra for the carbon supported samples containing platinum and Pt-Ru alloy catalysts are shown in Figures 10 and 11, respectively. Of these, only the carbon-supported platinum catalyst sample that was not subjected to heat treatment in a vacuum showed the presence of a paramagnetic resonance at  $g$  values of 2.0034 and 2.0026 at 30 °C (Figure 10a) and -140 °C (Figure 10b), respectively, similar to those reported for  $\text{Pt}^+$  by Huizinga and Prins,<sup>44</sup> no such paramagnetic platinum species could be detected after the sample had been heat treated in a vacuum (Figure 10c). The carbon-supported ruthenium and Pt-Ru alloy catalyst samples showed ESR signals with  $g$  values of 1.995 (Figure 11a) and 1.999 (Figure 11b); these  $g$  values are in the range reported for various  $\text{Ru}^{3+}$  compounds.<sup>16,45-47</sup>

We therefore conclude that the carbon-supported platinum catalysts contain oxidized-platinum impurities that are converted to elemental platinum in a reducing

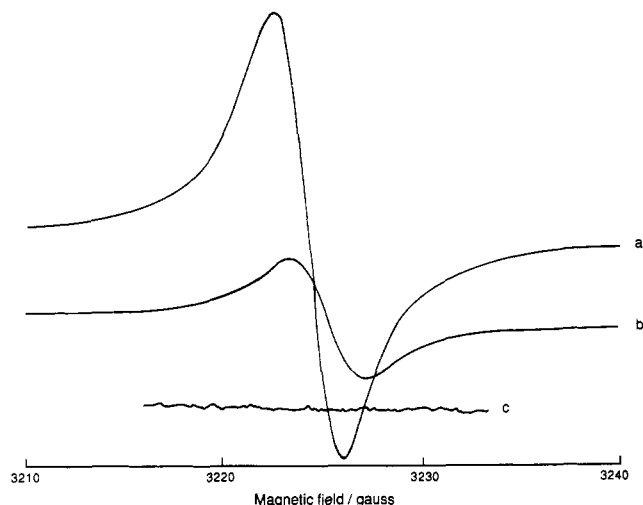


**Figure 10.** ESR spectra of (a) carbon-supported platinum at -140 °C, (b) carbon-supported platinum at 30 °C, and (c) after heat treatment in a vacuum at 500 °C.

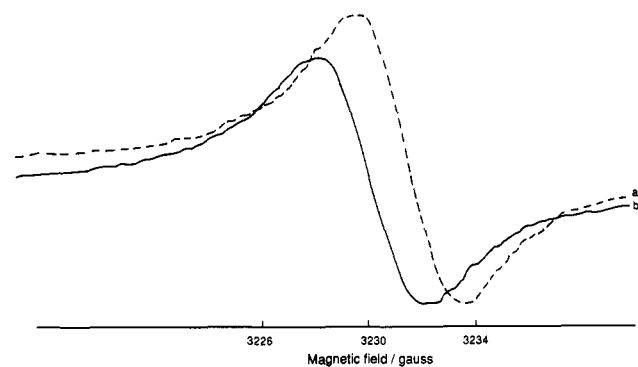


**Figure 11.** ESR spectra of (a) carbon-supported ruthenium at -140 °C and (b) carbon-supported 25-75 Pt-Ru alloy at -140 °C.

atmosphere. On the other hand, carbon-supported 25-75 Pt-Ru alloy catalysts do not contain any impurities of oxidized Pt even in the presence of oxides of ruthenium. One important effect of the Ru in the alloy is to scavenge oxygen species from the neighboring Pt atoms.

Average particle sizes of the catalysts were determined from the line broadening in the X-ray diffractograms and electron micrographs.<sup>16</sup> Pt/C gave sharp peaks, while Pt-Ru/C showed diffuse patterns characteristic of Pt-Ru alloy. The patterns were sharp enough to eliminate the possibility of two separate phases, and the peaks were shifted from the values of Pt. The Pt particle diameter on carbon was 20 nm, while the vacuum-annealed Pt on carbon had a 40-nm diameter. On the other hand, the Pt-Ru/C showed a particle diameter of less than 5 nm. It is also observed<sup>48,49</sup> that Pt forms a single-phase alloy with Ru to 83 at. % Ru. Hence, we may conclude that the Pt-Ru catalyst is present as extremely fine particles and as an alloy. We could not carry out a surface-segregation analysis of these Pt-Ru alloy particles; other workers<sup>5,6,50</sup> have found Pt enrichment on the surface of these alloys. According to this published data, 80-20, 70-30, and 45-55 Pt-Ru alloys prepared in bulk form from the melt have surface ratios 89-11, 80-20, and 65-35 Pt-Ru, respectively. We anticipate a much smaller surface segregation in our

(44) Huizinga, P.; Prins, R. *J. Phys. Chem.* **1983**, *87*, 173.

(45) Geschwind, S.; Remeika, J. P. *J. Appl. Phys.* **1962**, *33*, 370.

(46) Kamimura, H. *Phys. Rev.* **1968**, *128*, 269.

(47) Miller, I.; Offenbacher, E. L. *Phys. Rev.* **1968**, *166*, 269.

(48) Ross, P. N.; Kinoshita, K.; Scarpellino, A. J.; Stonehart, P. J. *Electroanal. Chem.* **1975**, *63*, 97.

(49) Bond, G. C.; Webster, D. E. *Ann. N.Y. Acad. Sci.* **1969**, *158*, 540.

(50) Hilaré, L.; Guerrero, G. D.; Legare, P.; Maine, G.; Krill, G. *Surf. Sci.* **1984**, *145*, 569.

fine particles prepared at room temperature.

The total surface area of Pt-Ru/C was  $1800 \text{ m}^2 \text{ g}^{-1}$  as determined from the nitrogen BET. The percent distribution of Pt, Ru, and Pt-Ru on carbon was found to be 77, 27, and 129, respectively. (The percent distribution is 100 times the ratio of the surface atoms of the catalyst, as estimated by hydrogen chemisorption, to the total number of atoms actually deposited onto a carbon support.) Maximum dispersion for Pt-Ru may be accounted for by the hydrogen spillover phenomenon. Robell et al.,<sup>51</sup> Boudart et al.,<sup>52</sup> and Bagotzky and Skundin<sup>53</sup> have also reported hydrogen spillover for Pt on carbon.

The 50-50 Ni-Ti alloy gave an X-ray diffraction pattern similar to that of Cr-Fe. The structure of this alloy changes with small departures from stoichiometry, and the stability of the alloy in the working electrolyte is only ensured at the 50-50 Ni-Ti composition. We therefore may assume that the surface composition is similar to that in the bulk.

### Conclusions

Anticipation of a net charge transfer from the more electropositive to the more electronegative partner of a binary alloy is supported by spectroscopic evidence from

(51) Robell, A. J.; Ballou, E. V.; Boudart, M. *J. Phys. Chem.* **1964**, *68*, 2748.

(52) Boudart, M.; Aldag, A. W.; Vannice, M. A. *J. Catal.* **1970**, *18*, 46.

(53) Bagotzky, V. S.; Skundin, A. M. *Electrochim. Acta* **1984**, *29*, 757.

the Pt-Ru system. Moreover, straightforward—though qualitative—arguments based on such a charge transfer are able to account satisfactorily for several features of the synergistic enhancement of activity on Pt-Ru alloys of three important fuel cell reactions. However, a relatively strong 3d-electron transfer from Ti to Ni, which is responsible for the stabilization of Ni-Ti in acid, binds surface species won from the electrolyte too strongly to permit fuel cell reactants access to the surface. Therefore, as anticipated, fuel cell reactions are suppressed at a Ni-Ti electrode. On the other hand, electrolytic reactions proceed normally—and stably in acid—on a Ni-Ti alloy, but the onset potentials and exchange-current densities are shifted by the bias fields introduced by charge transfer within the alloy.

These preliminary results must encourage the exploration of other alloy systems tailored to promote specific catalytic reactions.

**Acknowledgment.** Support of this work by the R. A. Welch Foundation, Houston, TX, and the Department of Non-Conventional Energy Sources, Ministry of Energy, Government of India, New Delhi, is gratefully acknowledged.

**Registry No.** Pt-Ru, 12779-05-4; O<sub>2</sub>, 7782-44-7; H<sub>2</sub>, 1333-74-0; CH<sub>2</sub>OH, 67-56-1; C, 7440-44-0; 50-50 Ni-Ti, 11110-85-3; 75-25 Pt-Ru, 37258-16-5; 40-60 Pt-Ru, 42615-02-1; 55-45 Pt-Ru, 50954-06-8; 70-30 Pt-Ru, 63627-81-6; 25-75 Pt-Ru, 121232-02-8; polyethylene, 9002-88-4.

## Formation of Particulate Opaque Silica Gels from Highly Acidic Solutions of Tetramethoxysilane

Hiromitsu Kozuka\* and Sumio Sakka

*Institute for Chemical Research, Kyoto University, Uji, Kyoto-Fu 611, Japan*

*Received October 13, 1988*

The gelation behavior of highly acidic solutions of tetramethoxysilane (TMOS) of molar compositions  $\text{TMOS:H}_2\text{O:CH}_3\text{OH:HCl} = 1:1.44\text{--}2.00:2:0.01\text{--}0.40$  has been studied. The most weakly acidic solutions ( $\text{HCl/TMOS} = 0.01$ ) turned into spinnable sols and then transformed into transparent gel fragments, whereas solutions of higher HCl content did not show spinnability and lost their transparency before gelation. The gels derived from highly acidic solutions were of a particulate nature, consisting of distinct large particles. A gel monolith consisting of 5- $\mu\text{m}$  particles was obtained from the solution of  $\text{TMOS:H}_2\text{O:CH}_3\text{OH:HCl} = 1:1.53:2:0.40$ .

### Introduction

Synthesis of silica glass by the sol-gel method consists of (1) gel formation through hydrolysis and polycondensation reaction of silicon alkoxide, (2) drying of the wet gel, and (3) transformation of the dried gel into silica glass by sintering. This route for preparing silica glass is attractive since this makes it possible to prepare shaped silica glasses at low temperatures without melting. To make bulk silica gel, precursor for bulk silica glass, fracture of the gel during the drying process should be avoided. Crack formation during drying may be caused by the stress generated in the gel due to capillary forces, and hence it is assumed that the fracture may be suppressed by making gels having continuous pores of large size. Rabinovich et al.<sup>1,2</sup> have prepared gels with a two-mode pore-size dis-

tribution, one maximum in the region 1-8  $\mu\text{m}$  and the other in the region 13-20 nm, by dispersing dense gels in water with a high-shear device. Scherer and Luong<sup>3</sup> have prepared silica particles of 60-100 nm in diameter by flame oxidation of  $\text{SiCl}_4$  and dispersed them in organic liquids with the additions of alcohol, producing gelation by adding amines or ammonia. Prassas et al.<sup>4</sup> have prepared gels with a porous microstructure by heating sols in the autoclave prior to gelation. Another method for making crack-free

(1) Rabinovich, E. M.; Johnson Jr., D. W.; MacChesney, J. B.; Vogel, E. M. *J. Am. Ceram. Soc.* **1983**, *66*, 683.

(2) Rabinovich, E. M. *J. Mater. Sci.* **1985**, *20*, 4259.

(3) Scherer, G. W.; Luong, J. C. *J. Non-Cryst. Solids* **1984**, *63*, 163.

(4) Prassas, M.; Phalippou, J.; Zarzycki, J. *J. Mater. Sci.* **1984**, *19*, 1656.